Single-Atom Anchored Magnetic Nanocomposites for Simultaneous Adsorption and In-Situ Photocatalytic Reduction of Toxic Oxyanions [Cr(VI)/As(V)]

Dr. Vikas Nain

PhD in Chemistry
Email id: vnain008@gmail.com

Abstract

Hexavalent chromium and arsenate are persistent oxyanion contaminants whose remediation is complicated by high aqueous mobility, redox-sensitive speciation, and interference from common groundwater ions. This manuscript proposes a bifunctional magnetic photocatalyst in which atomically dispersed Fe sites (nominally Fe–N_4 motifs) are anchored on nitrogen-rich graphitic carbon nitride and coupled to Fe_3O_4 nanoparticles, abbreviated FeSA–CN/Fe_3O_4. The design integrates three functions in one recoverable solid: electrostatic/inner-sphere enrichment of oxyanions, single-atom-mediated interfacial electron transfer, and magnetically assisted catalyst separation. Under visible light, electrons promoted to the carbon-nitride conduction band are funneled through isolated Fe sites and the magnetite-containing interface toward adsorbed Cr(VI) or As(V). For chromium, the target chemistry is reduction to Cr(III), followed by surface complexation or precipitation. For arsenic, reduction must not be allowed to terminate at As(III), which can be more mobile and hazardous; the scientifically relevant reductive endpoint is immobilized elemental As(0), requiring strongly electron-rich, low-oxygen conditions and efficient hole scavenging. The proposed workflow therefore separates dark adsorption from illuminated redox tests, quantifies aqueous and surface speciation, and explicitly evaluates dissolved oxygen as a competing electron sink. Adsorption is interpreted with equilibrium and kinetic models, whereas photoreduction is assessed by apparent pseudo-first-order kinetics, product speciation, iron leaching, magnetic recovery, and multi-cycle stability. Published studies on Fe-coordinated carbon nitride, magnetic g-C_3N_4 composites, and single-atom photocatalysts establish the plausibility of each design element. The resulting framework provides a chemically defensible route for testing whether atomic-site engineering and magnetic recovery can convert a conventional adsorbent–photocatalyst into a selective, reusable platform for mixed Cr(VI)/As(V) treatment.

Keywords: single-atom catalyst; Fe–N_4; magnetic nanocomposite; graphitic carbon nitride; Cr(VI); As(V); adsorption; photocatalytic reduction; speciation; water treatment

1. Introduction

Chromium and arsenic contamination remains a demanding problem in industrial effluents, mining-impacted water, metallurgical drainage, and geogenic groundwater because their environmental behavior depends not only on total concentration but also on oxidation state. In oxic aqueous systems, Cr(VI) commonly occurs as $HCrO_4^-$, CrO_4^{2-}, or $Cr_2O_7^{2-}$ according to pH and concentration; these anionic forms are comparatively mobile and strongly oxidizing. Reduction to Cr(III) changes the treatment problem from a mobile oxyanion to a cationic/hydrolyzed species that can bind strongly to oxide surfaces or precipitate as hydroxide phases. Consequently, a material that first concentrates Cr(VI) at an interface and then supplies photogenerated electrons at that same interface can couple mass transfer with detoxification rather than treating adsorption and redox as separate unit operations [7–11,13].

Arsenic is more complicated. Arsenate, As(V), is usually present as $H_2AsO_4^-$ or $HAsO_4^{2-}$ in the circumneutral pH region, whereas As(III) is dominated by weakly charged or neutral arsenous-acid species. Many practical photocatalytic arsenic systems therefore operate oxidatively: As(III) is converted to As(V), which is then captured by iron- or aluminum-containing surfaces [3–6]. The present title, however, specifically requires photocatalytic reduction of As(V). Early TiO_2 photoredox work demonstrated that adsorbed As(V) can indeed accept

photogenerated electrons and, under acidic deoxygenated conditions with a hole scavenger, can proceed toward elemental arsenic [1]. Later photoelectrochemical studies confirmed that As(V) reduction is strongly suppressed by dissolved oxygen because O_2 is a kinetically efficient electron acceptor [2]. These findings impose a crucial design rule: a reductive As(V) process is only defensible if the reactor is operated to avoid accumulation of As(III) and to verify formation/retention of As(0) or another immobilized reduced product.

Graphitic carbon nitride (g-C_3N_4) is attractive for visible-light water treatment because its conjugated heptazine network supports photoexcitation without precious metals and offers nitrogen sites capable of coordinating transition metals. Its limitations—moderate charge-carrier recombination, imperfect interfacial adsorption, and powder recovery—can be addressed through atomic-site engineering and magnetic integration. Fe-coordinated g-C_3N_4 has already been shown to promote Cr(VI) photoreduction, including the kinetically important conversion of Cr(V) intermediates to Cr(III) [11]. Independent single-atom studies show that isolated Fe–N_4-like centers on carbon nitride can accelerate interfacial electron transfer and stabilize reactive coordination environments [10,12,16]. Magnetic Fe_3O_4/g-C_3N_4 composites, meanwhile, provide straightforward solid recovery and can improve electron transport or adsorption [7–9].

1.1 Objectives of the study

1. To synthesize and optimize magnetic nanocomposites containing uniformly dispersed single metal atoms as highly active adsorption and photocatalytic sites.
2. To characterize the prepared nanocomposites for their structural, morphological, surface, optical, magnetic, and chemical properties using suitable analytical techniques such as XRD, SEM/TEM, XPS, BET, FTIR, UV–Vis DRS, and VSM.
3. To investigate the adsorption behaviour of Cr(VI) and As(V) on the developed material under different experimental conditions, including pH, contact time, initial oxyanion concentration, adsorbent dosage, temperature, and competing ions.
4. To evaluate the photocatalytic reduction efficiency of Cr(VI) under visible or solar-light irradiation and determine the role of single-atom active sites in improving charge separation and electron-transfer processes.
5. To examine the light-assisted transformation and immobilization of As(V) and determine whether photocatalytic conversion enhances its subsequent adsorption or removal by the magnetic nanocomposite.

2. Scientific Premise and Nanocomposite Design

The proposed composite is deliberately modular. The photocatalytic scaffold is nitrogen-rich g-C_3N_4, preferably prepared with controlled nitrogen vacancies or a porous morphology to expose coordination sites without excessively narrowing the electronic structure. A low loading of Fe precursor is introduced so that Fe atoms can be stabilized by pyridinic/heptazinic N atoms as isolated coordination centers rather than forming metallic or oxide clusters. These FeSA sites are expected to function as localized electron-accepting/donating centers that modify the density of states near the carbon-nitride framework, strengthen oxyanion adsorption where electrostatics and ligand exchange are favorable, and accelerate transfer of conduction-band electrons to reducible species. The concept is consistent with single-atom Fe–N coordination on carbon nitride reported for photocatalytic redox systems and with the growing use of atomically dispersed Fe as a tunable interfacial catalyst [10,12,16].

Fe_3O_4 is introduced as a physically distinguishable magnetic phase, ideally as 10–50 nm nanoparticles deposited after the Fe single-atom anchoring step or attached through a thin carbonaceous/polydopamine-derived interlayer. The sequencing matters: co-pyrolysis of all Fe species risks converting the intended FeSA population into clusters or nanoparticles, making the phrase “single-atom anchored” analytically indefensible. A low-temperature assembly route is therefore preferred after single-atom formation. Magnetite offers a high magnetic response for separation, Fe–OH surface groups for oxyanion association, and mixed-valence Fe(II)/Fe(III) character that may facilitate interfacial electron transport. However, magnetite cannot be treated as an innocent support; its contribution must be isolated through Fe_3O_4-only and g-C_3N_4/Fe_3O_4 controls.

Table 1. Component–function relationships and required evidence for the proposed FeSA–CN/Fe_3O_4 system.

Component / motif	Primary chemical function	Expected evidence	Critical control
N-rich g-C_3N_4	Visible-light absorption; electron–hole generation; N coordination matrix.	UV–Vis DRS band edge; XRD/FTIR heptazine signatures; PL/TRPL charge dynamics.	Pristine g-C_3N_4 under identical adsorption and illumination conditions.
Isolated Fe–N_x site	Electron-transfer mediator; local coordination/adsorption center; possible Cr(V)→Cr(III) acceleration.	Atomic HAADF-STEM spots without Fe lattice fringes; Fe 2p XPS; XANES/EXAFS showing Fe–N coordination and negligible Fe–Fe path.	Same g-C_3N_4 with no FeSA; plus a deliberately clustered-Fe comparator if feasible.
Fe_3O_4 nanoparticle	Magnetic recovery; oxide adsorption sites; mixed-valence electron relay.	XRD/Raman magnetite phase; VSM hysteresis; Fe 2p; TEM particle size and spatial separation from isolated FeSA motifs.	Fe_3O_4 alone and g-C_3N_4/Fe_3O_4 without atomically dispersed Fe.
Interfacial linker / carbon layer	Improves mechanical attachment and electron percolation; may add adsorption sites.	C 1s/N 1s changes; Raman; TEM interface continuity; electrochemical impedance.	Composite prepared without linker to distinguish electronic from adsorption effects.
Adsorbed Cr/As oxyanion	Creates surface-confined electron-acceptor complex prior to irradiation.	Dark uptake; zeta potential; Cr/As XPS; As K-edge or Cr K-edge XANES where accessible.	Light-only, dark-only, and no-catalyst blanks; competing-ion tests.

2.1 Selectivity logic

At acidic pH, protonation of surface N/O groups increases attraction toward chromate and arsenate oxyanions. Adsorption is expected to be strongest when electrostatic attraction is supplemented by inner-sphere complexation on Fe-containing sites. This preconcentration is useful only if the subsequent electron-transfer pathway is selective enough to compete with dissolved oxygen, nitrate, natural organic matter, and other electron sinks. Thus, "simultaneous adsorption and reduction" should be demonstrated by time-resolved mass balances and valence-state analysis rather than by a single decline in dissolved total Cr or total As.

3. Proposed Materials and Methods

3.1 Synthesis of Fe single-atom carbon nitride

A representative synthesis can begin with melamine or urea as the carbon-nitrogen precursor. The precursor is mixed with a dilute Fe chelate (for example, an Fe(III) salt complexed with a nitrogen-rich ligand) at a loading low enough to favor atomic dispersion. After drying, the solid is thermally condensed under N_2 using a staged program in the approximate 500–550 °C range. The goal is not maximum Fe loading but maximum fraction of isolated Fe–N_x environments. A post-synthetic acid wash may remove weakly bound Fe clusters, followed by repeated washing to neutral pH and vacuum drying. The Fe content should be quantified by ICP-OES or ICP-MS so that photocatalytic activity can be normalized both to catalyst mass and to Fe content. A parallel Fe-free g-C_3N_4 batch must be prepared using the identical thermal history.

3.2 Magnetic integration

Fe_3O_4 nanoparticles can be synthesized separately by alkaline co-precipitation of Fe(II)/Fe(III) salts under inert gas, washed until low ionic conductivity is reached, and then immobilized onto FeSA–CN by sonication-assisted assembly. To reduce nanoparticle detachment, a nanometric carbonaceous or polydopamine-derived linker can be introduced at low loading; the final annealing temperature should be sufficiently mild to preserve Fe_3O_4 and avoid migration of FeSA into clusters. A target Fe_3O_4 fraction of roughly 10–30 wt% is a reasonable screening range because it balances magnetic response against optical shielding. This is a proposed optimization window, not a

claimed optimum. Magnetic separation should be quantified by recovery yield after a defined magnet exposure time rather than described qualitatively.

3.3 Structural and electronic characterization

Convincing proof of a single-atom architecture requires multiple complementary methods because the composite intentionally contains both atomic Fe and Fe_3O_4. Powder XRD should identify g-C_3N_4 and magnetite while the absence of a diffraction peak from a dilute FeSA population is expected but not sufficient evidence for atomic dispersion. Aberration-corrected HAADF-STEM can visualize isolated high-Z Fe spots on the carbon-nitride support; statistical image analysis should also check for sub-nanometer clusters. XPS resolves surface Fe, N, C, Cr, and As states, but XPS alone cannot prove single-atom dispersion. Fe K-edge XANES/EXAFS is therefore the preferred ensemble-level evidence: a dominant Fe–N first shell combined with a negligible Fe–Fe scattering path would support isolated Fe, whereas magnetite contributes Fe–O/Fe–Fe paths that should be deconvoluted using physically meaningful reference spectra. Mössbauer spectroscopy is highly valuable if available because it can separate magnetic oxide Fe from distinct FeSA electronic environments.

Optical and charge-transport characterization should include diffuse-reflectance UV–Vis spectroscopy, steady-state and time-resolved photoluminescence, photocurrent response, and electrochemical impedance spectroscopy. Radical or charge-carrier trapping experiments are secondary evidence and must not substitute for direct metal-speciation analysis. Surface area and pore structure should be obtained by N_2 sorption, while zeta potential as a function of pH provides a practical map for oxyanion adsorption. Vibrating-sample magnetometry confirms that the final composite remains magnetically recoverable after photocatalytic cycling.

3.4 Adsorption experiments and equilibrium analysis

Dark adsorption must be measured before illumination so that true photochemical conversion is not conflated with simple uptake. Batch tests should use acid-washed glassware or validated polymer vessels, a fixed solution-to-solid ratio, and independently prepared Cr(VI) and As(V) stock solutions. Screening across pH 2–9 should be followed by focused kinetic and equilibrium studies within the pH region that maintains catalyst stability and favors the intended oxyanion speciation. Cr(VI) can be monitored colorimetrically with 1,5-diphenylcarbazide for rapid screening, while total Cr and total As should be confirmed by ICP-OES/ICP-MS. Arsenic speciation requires a separation method such as HPLC-ICP-MS or validated selective hydride-generation protocols because total As alone cannot distinguish As(V), As(III), and any dissolved reduced intermediate.

$$q_e = ((C_0 - C_e)V) / m \quad (1)$$

Equilibrium adsorption capacity, where C_0 and C_e are initial/equilibrium concentrations, V is solution volume, and m is catalyst mass.

$$q_e = (q_{max}\, K^L\, C_e) / (1 + K^L\, C_e) \quad (2)$$

Langmuir model for a finite population of adsorption sites; parameter interpretation should be supported by residual analysis, not R^2 alone.

$$t/q_t = 1/(k_2\, q_e^2) + t/q_e \quad (3)$$

Linearized pseudo-second-order kinetic expression; nonlinear fitting is preferred for final parameter estimation.

Table 2. Proposed experimental matrix for separating adsorption, photoredox chemistry, and matrix effects.

Experiment	Core condition	Primary response	Purpose
Dark adsorption	No light; pH 2–9; single and mixed oxyanions	q_t, q_e, zeta potential, dissolved Cr/As	Quantify preconcentration and competition before photochemistry.
Photolysis blank	Light; no catalyst	Cr(VI), As(V), total Cr/As	Exclude direct photolysis or reactor-wall effects.
Photocatalysis	Visible light; catalyst; controlled O_2	Speciation vs time; k_app	Resolve light-driven reduction after adsorption equilibrium.

Oxygen series	N_2/Ar purge vs air-saturated vs O_2-rich	As(V)/As(III)/As(0) balance; Cr species	Test electron competition by O_2, especially for As(V).
Hole-scavenger series	0–defined organic donor concentration	Reduction rate; donor consumption; TOC	Determine whether enhanced electron availability drives complete reduction.
Co-ion challenge	SO_4^{2-}, NO_3^-, HCO_3^-, PO_4^{3-}, Cl^-, DOM	Selectivity, rate suppression, desorption	Assess realistic water-matrix sensitivity.
Reuse / leaching	≥5 separation–wash–reuse cycles	Activity retention; Fe loss; magnetization	Verify recoverability and structural stability.

3.5 Adsorption controls and mass balance

After dark equilibration, both supernatant and solid should be retained. Aqueous mass loss is only the first term in a mass balance; desorption tests, acid digestion of the recovered catalyst, and surface spectroscopy are required to confirm where Cr or As resides. Mixed Cr(VI)/As(V) experiments should be performed only after single-solute adsorption envelopes are established, because phosphate and arsenate in particular can compete strongly for Fe–OH-type sites. Report adsorption capacities both per gram of total composite and, where informative, per unit surface area to distinguish improved chemistry from simple surface-area changes.

3.6 Photocatalytic reduction protocol

Photocatalytic experiments should begin only after a reproducible dark adsorption period. A visible-light source with a defined cutoff (for example, $\lambda > 420$ nm) is preferable to an unspecified lamp because spectral overlap controls carrier generation. Photon flux should be measured using a calibrated radiometer or chemical actinometer, and reactor temperature should be held constant to avoid confusing thermal effects with photocatalysis. The suspension is mixed continuously but gently enough to prevent excessive catalyst attrition. Aliquots are removed through a validated low-adsorption filter or after rapid magnetic separation, then immediately stabilized for metal-speciation analysis.

Two atmosphere modes are required. Cr(VI) reduction can be studied under both air-equilibrated and low-oxygen conditions to quantify the penalty associated with oxygen reduction. The As(V) reduction experiment, by contrast, should be conducted under N_2 or Ar with verified dissolved oxygen below a defined threshold. A sacrificial hole donor may be screened only as a mechanistic tool and should not be presented as a practical water-treatment reagent without assessing residual organic carbon and by-products. The key endpoint is a closed arsenic mass balance showing whether As(V) disappeared by adsorption, converted transiently to As(III), or accumulated as a surface-bound As(0)-like product.

$$\textbf{Removal (\%)} = 100 \times (C_0 - C_t)/C_0 \quad (4)$$

This metric is useful for process performance but is not sufficient to prove reduction or detoxification.

$$\ln(C_0/C_t) = k_{app}\, t \quad (5)$$

Apparent pseudo-first-order representation used only over the time interval where the model is statistically appropriate.

$$\textbf{AQY (\%)} = 100 \times \textbf{(electrons consumed in target reduction)/(incident photons)} \quad (6)$$

An apparent quantum yield can compare electron use efficiency when photon flux and product stoichiometry are measured.

3.7 Speciation-resolved analytical plan

Cr(VI) should be quantified separately from total chromium. The difference between total Cr and Cr(VI) in solution can suggest formation of Cr(III), but a rigorous assignment should also use XPS or Cr K-edge XANES on the recovered solid because Cr(III) may adsorb immediately after reduction. For arsenic, total As and chromatographically resolved As(V)/As(III) should be measured at each time point. Surface XPS can detect shifts consistent with reduced As, while As K-edge XANES/EXAFS provides stronger oxidation-state and coordination evidence if available. Any claim of As(0) formation should be based on at least two independent lines of evidence,

because surface charging and spectral overlap can complicate XPS interpretation.

3.8 Statistics, reproducibility, and kinetic comparison

Each condition should include at least triplicate independent reactor runs and a mass-balance check. Report means with standard deviations or confidence intervals, but also show individual replicate points in supplementary datasets. Model fitting should be nonlinear wherever possible, with Akaike information criterion or residual analysis used to compare kinetic/isotherm models. When comparing composites, normalize light intensity, catalyst dose, target concentration, and exposed reactor geometry. Cross-paper "percent removal" values should be treated as qualitative benchmarks because those variables differ substantially among studies.

3.9 Safety and waste control

Cr(VI), arsenate, arsenite, and any reduced arsenic-bearing solid must be handled as hazardous toxic-metal waste. Experiments require a certified chemical fume hood, appropriate gloves and eye protection, dedicated metal-contaminant labware, secondary containment, and institution-approved disposal. Photocatalyst powders should be handled to minimize inhalation. Reduced products must not be released merely because aqueous concentrations decrease; the recovered catalyst and all regeneration eluates remain hazardous until stabilized and disposed through an authorized route.

4. Coupled Adsorption–Photoredox Mechanism

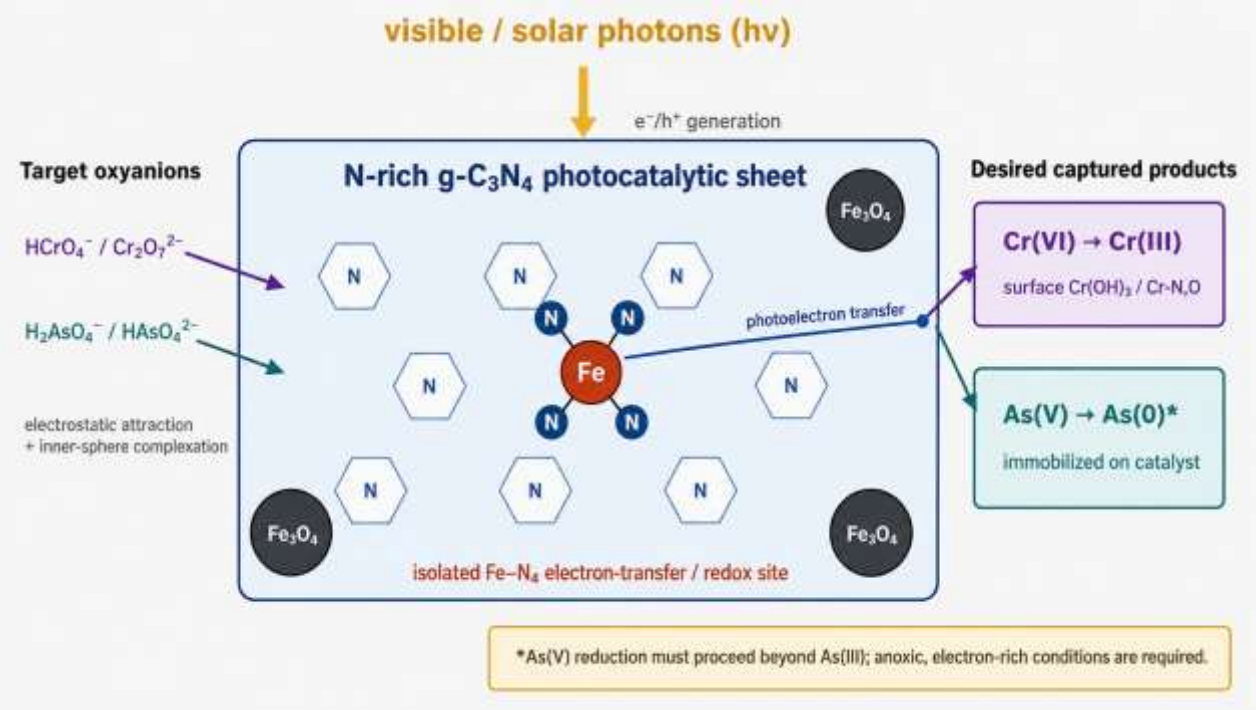

Figure 1. Proposed architecture of FeSA–CN/Fe₃O₄. Oxyanions are enriched at N/Fe-containing interfaces, while visible-light excitation supplies electrons to Fe single-atom sites and the magnetite-containing interface. The arsenic pathway is deliberately drawn toward immobilized As(0), because stopping at As(III) is not a safe reductive endpoint.

The mechanistic sequence begins in the dark. Protonated edge N sites and hydroxylated Fe-containing surfaces attract chromate and arsenate electrostatically, while ligand exchange can create stronger inner-sphere complexes. Once illumination begins, g-C_3N_4 generates electron–hole pairs. Isolated Fe–N_x sites can trap or mediate electrons at energies that favor interfacial transfer, whereas Fe_3O_4 and a conductive carbonaceous linker can shorten the distance between the semiconductor and adsorbed acceptors. This does not imply that every Fe atom has the same role: magnetite Fe contributes magnetic and oxide-surface chemistry, while the atomically dispersed Fe population is

hypothesized to control local electronic activation. The distinction should be tested by phase-specific spectroscopy and component controls.

For Cr(VI), electron transfer to protonated chromate species is thermodynamically favorable in acidic media and proceeds through lower-valent chromium intermediates. Recent Fe-coordinated carbon-nitride work highlights Cr(V)→Cr(III) as a kinetically consequential step that can be accelerated by Fe coordination [11]. Once formed, Cr(III) can remain associated with the composite through hydrolysis, complexation, or precipitation depending on pH. Therefore, a decline in Cr(VI) together with retained total Cr on the solid is mechanistically compatible with sequential adsorption–reduction–immobilization rather than simple desorption.

4.1 Electron-transfer scheme and redox stoichiometry

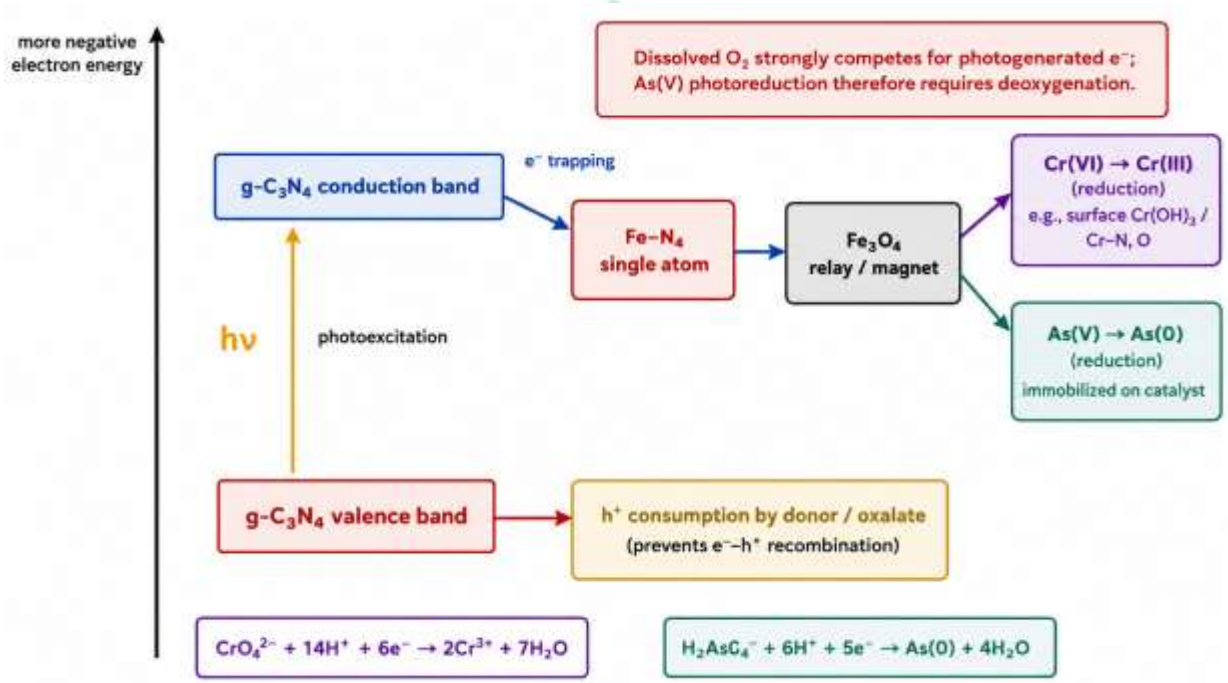

Figure 2. Conceptual electron-transfer map. Photoexcited g-C_3N_4 supplies conduction-band electrons to FeSA/Fe_3O_4-associated sinks; holes are consumed by water or a mechanistic hole donor. Oxygen is shown as a competing electron acceptor because it can suppress As(V) reduction.

$$Cr_2O_7^{2-} + 14H^+ + 6e^- \rightarrow 2Cr^{3+} + 7H_2O \quad (7)$$

$$HCrO_4^- + 7H^+ + 3e^- \rightarrow Cr^{3+} + 4H_2O \quad (8)$$

$$H_2AsO_4^- + 6H^+ + 5e^- \rightarrow As(0) + 4H_2O \quad (9)$$

Equations (7)–(9) express formal half-reactions and should not be interpreted as evidence that a single elementary step transfers three, five, or six electrons. Surface photoredox reactions are expected to proceed through sequential electron/proton transfers and adsorbed intermediates. In chromium reduction, Cr(V) and Cr(IV) intermediates may be short-lived or surface-confined. In arsenic reduction, As(III) is a chemically plausible intermediate even when the desired final product is As(0). Time-resolved speciation is therefore essential: a transient rise in As(III) followed by its decline as solid-phase reduced arsenic increases would support a stepwise pathway; persistent As(III) accumulation would falsify the "safe reductive immobilization" hypothesis.

4.2 Role of pH and surface charge

Acidic conditions favor both proton-assisted reduction and positive surface charge on many N/O-containing interfaces, which can increase oxyanion adsorption. Yet very low pH can also dissolve Fe species, destabilize magnetite, and change the surface coordination environment. The optimum pH must therefore satisfy three constraints simultaneously: adsorption, redox kinetics, and catalyst stability. A practical study should report the final pH as well as the initial pH because proton-consuming reduction and buffer chemistry can shift the reaction environment during irradiation.

4.3 Electron competition and hole management

Electron selectivity can be expressed conceptually as competition among adsorbed Cr(VI), adsorbed As(V),

dissolved O_2, and other reducible solutes. Raising the local coverage of the target oxyanion through adsorption is one route to favor target electron transfer. A second route is kinetic gating at FeSA coordination sites, where adsorption geometry may position an oxyanion close to accumulated charge. A third is control of the hole side of the reaction: efficient hole consumption suppresses recombination and increases the electron population available for reduction. These strategies must be evaluated together, because a catalyst with excellent light absorption can still be ineffective if target adsorption is weak or O_2 captures most electrons.

5. Literature-Grounded Expected Results and Discussion

5.1 Cr(VI): expected adsorption–reduction behavior

Published magnetic g-C_3N_4 systems establish that coupling carbon nitride with Fe_3O_4-containing phases can substantially improve Cr(VI) treatment. Ding et al. reported a Fe_3O_4/C/g-C_3N_4 composite whose observed Cr(VI) photoreduction rate constant was markedly higher than that of pristine g-C_3N_4, with the carbon/Fe_3O_4 interface assisting both adsorption and electron transport [7]. Wang et al. further showed that a ternary Fe_3O_4/g-C_3N_4/carbon composite combined ion exchange, reduction, and Cr(III) complexation and retained magnetic regeneration capability [8]. A Z-scheme Fe_3O_4/TiO_2/g-C_3N_4 composite later achieved high Cr(VI) removal under visible light while remaining magnetically separable [9]. These studies support the magnetic and interfacial elements of the present design, although none alone proves a single-atom mechanism. The single-atom contribution is supported by a different body of evidence. Fe–N_4-type sites on carbon nitride can reorganize charge transfer and promote reductive chemistry [10,12]. For Cr(VI) specifically, Fe coordination on g-C_3N_4 has been reported to improve removal and accelerate the conversion of Cr(V) to Cr(III), identifying an atomically localized Fe environment as more than a passive adsorption site [11]. More recently, post-synthetically introduced Fe single atoms in a Zr-based MOF produced rapid Cr(VI) photoreduction and were interpreted by experiment and computation as facilitating electron transfer to chromium species [13]. These results justify the expectation that FeSA–CN/Fe_3O_4 should outperform an Fe-free magnetic carbon nitride control when normalized to absorbed photons and accessible surface area.

5.2 What a convincing Cr(VI) result would look like

A convincing data set would show a fast initial decline in aqueous Cr(VI) during dark equilibration, followed by an additional light-dependent decrease accompanied by growth of Cr(III) signatures on the recovered solid. The photochemical enhancement should disappear or weaken when light is removed, when FeSA is omitted, or when an electron scavenger is added. The FeSA-containing material should also exhibit lower photoluminescence intensity/longer useful carrier lifetime or higher photocurrent relative to the FeSA-free analogue, but such electronic signals should be correlated with chemistry rather than treated as proof by themselves. If total dissolved chromium falls but surface spectroscopy shows only Cr(VI), then the dominant mechanism is adsorption and the photoreduction claim is unsupported.

5.3 Kinetic interpretation

An apparent first-order rate constant is useful for within-study comparisons only when initial concentration, catalyst dose, light flux, reactor geometry, and oxygen conditions are constant. A stronger analysis would compare the initial electron-equivalent removal rate and apparent quantum yield. Because Cr(VI) reduction consumes multiple electrons, product-selective electron accounting can reveal whether a faster concentration decrease actually reflects improved charge utilization. In mixed Cr(VI)/As(V) solutions, Cr(VI) may dominate electron capture under some conditions; therefore, individual and mixed-solute kinetic constants should be reported together with time-dependent speciation rather than summarized as a single “total removal” percentage.

5.4 Surface transformation after chromium reduction

Formation of Cr(III) can alter the catalyst itself. Hydrolyzed Cr(III) may occupy Fe–OH or N-containing sites, change zeta potential, block pores, or create mixed Fe–Cr surface phases after repeated cycles. Regeneration protocols should therefore be selected with care: aggressive acid can recover adsorption capacity but may leach Fe or destroy FeSA coordination, whereas mild chelation may remove Cr(III) more selectively but create a contaminated regenerant stream. Reuse results should be interpreted together with post-cycle XPS/XANES, ICP-measured Fe loss, and

magnetization changes.

5.5 As(V): expected behavior and the "As(III) trap"

The arsenic part of the study demands a different success criterion from chromium. Photocatalytic arsenic literature has largely favored oxidation of As(III) to As(V) followed by adsorption, because As(V) binds more strongly to many metal-(hydr)oxide surfaces [3–6]. Magnetic BiOI/γ-Fe_2O_3, for example, couples photocatalytic oxidation with oxide adsorption, while carbon-doped TiO_2/nitrogen-deficient C_3N_4 heterojunctions have achieved rapid As(III) oxidation and high total arsenic removal [5,6]. Those systems are useful benchmarks for integrated adsorption–photocatalysis, but their redox direction is opposite to the As(V) reduction requested here. For reductive operation, Yang et al. demonstrated that TiO_2 conduction-band electrons can reduce As(V) under acidic, deoxygenated conditions with a hole scavenger and observed elemental arsenic formation [1]. Monllor-Satoca et al. later showed that As(V) reduction on illuminated TiO_2 electrodes is concentration- and atmosphere-dependent and that oxygen strongly competes for photogenerated electrons [2]. The proposed FeSA–CN/Fe_3O_4 material should therefore be judged by whether it improves this difficult electron-transfer pathway while retaining reduced arsenic at the solid. A mere decrease in As(V) is ambiguous: it may reflect adsorption, partial conversion to soluble As(III), or true reduction to a less mobile As(0)-like product.

5.6 Expected signature of successful As(V) immobilizing reduction

Under N_2/Ar, an expected sequence is: rapid dark uptake of As(V); a light-induced transient increase in As(III) if the pathway is stepwise; subsequent decline of dissolved As(III) as reduced arsenic accumulates on the solid; and an increasing low-valent As signature in surface-sensitive spectroscopy. The total arsenic mass balance should remain near closure. If oxygen is introduced, the rate should fall sharply because O_2 diverts electrons; this oxygen-switch experiment is one of the strongest mechanistic controls available. If As(III) persists in the aqueous phase, the reductive mode should be considered unsuccessful from a treatment standpoint even if As(V) conversion is high.

5.7 Simultaneous Cr(VI)/As(V) treatment

"Simultaneous" treatment introduces both adsorption competition and redox competition. Chromate and arsenate can compete for positively charged or Fe–OH-type sites, while their electron-transfer kinetics and proton requirements differ. A robust mixed-solute study should construct a two-dimensional concentration matrix rather than test a single equimolar mixture. Time-resolved data can then reveal whether one oxyanion suppresses the other at the adsorption stage, the electron-transfer stage, or both. Selectivity factors based on adsorbed amount and electron-normalized reduction rate are more informative than total removal alone. One possible operating strategy is sequential selectivity within a single catalyst: use a dark contact period to preconcentrate both oxyanions, illuminate under conditions optimized for Cr(VI) reduction, then switch to more strongly reducing/deoxygenated conditions only if arsenic remains securely adsorbed and if As(III) does not accumulate. This is still "in-situ" chemistry on the same solid, but it avoids assuming that one atmosphere and one pH are optimal for two very different redox couples. Whether a truly one-stage condition exists should be an experimental result, not a premise.

5.8 Representative literature benchmarks

Table 3 places the proposed system against representative published studies. The values should not be ranked as if they were obtained under identical conditions: initial contaminant concentration, pH, catalyst dose, irradiation spectrum, oxygen level, and treatment time differ. Their value is mechanistic. Together they show that magnetic recovery, carbon-nitride photocatalysis, Fe coordination, and atomically dispersed Fe can each improve one component of the desired function. The research gap is to combine those elements while proving oxidation-state-resolved outcomes for both Cr and arsenic.

Table 3. Selected primary literature supporting the design rationale and performance envelope.

System / study	Target & reported result	Mechanistic relevance	Ref.
Fe_3O_4/C/g-C_3N_4	Cr(VI); k_obs reported 20.9× pristine g-C_3N_4.	Magnetic recovery plus adsorption/electron transport synergy.	[7]

Fe_3O_4/g-C_3N_4/C	Cr(VI); adsorption capacity 50.09 mg g^{-1}.	Ion exchange → reduction → Cr(III) complexation; reusable magnetic solid.	[8]
Fe_3O_4/TiO_2/g-C_3N_4	Cr(VI); ~95.6% removal under study conditions.	Visible-light Z-scheme behavior with magnetic separation.	[9]
Fe-coordinated g-C_3N_4	Cr(VI); removal increased up to 85.6% in reported series.	Fe coordination promotes Cr(V)→Cr(III), a key kinetic step.	[11]
Fe-DUT-67 single-atom catalyst	Cr(VI); 90% reduction in 18 min.	Direct single-atom Fe example for rapid Cr(VI) electron transfer.	[13]
BiOI/γ-Fe_2O_3 core–shell	As(III); 99.8% removal in 180 min.	Magnetic photocatalysis + adsorption; oxidative arsenic benchmark.	[5]
C/TiO_2@ND-C_3N_4	As(III); 95.0% total As removal; complete oxidation in 12 min.	Coupled photocatalytic oxidation and adsorption; shows value of tandem design.	[6]
TiO_2 (deoxygenated, hole scavenger)	As(V); elemental As observed.	Foundational evidence that photogenerated electrons can drive As(V) beyond As(III).	[1]

5.9 Expected benefit of atomic-site engineering

The main performance gain sought from FeSA is not simply higher adsorption capacity. A single atom coordinated by several N atoms creates a chemically defined site whose electronic structure can differ sharply from bulk iron oxides. Such sites can couple local adsorption geometry to carrier trapping and transfer, potentially raising the fraction of photogenerated electrons that reach an oxyanion before recombination. This hypothesis is testable by comparing FeSA–CN/Fe_3O_4 against g-C_3N_4/Fe_3O_4 at matched surface area and magnetite content, then normalizing reduction rates to photon flux. If the FeSA version shows only a higher dark uptake but no higher photon-normalized reduction rate, the data would support an adsorption role rather than a catalytic electron-transfer role.

5.10 Cross-study performance context

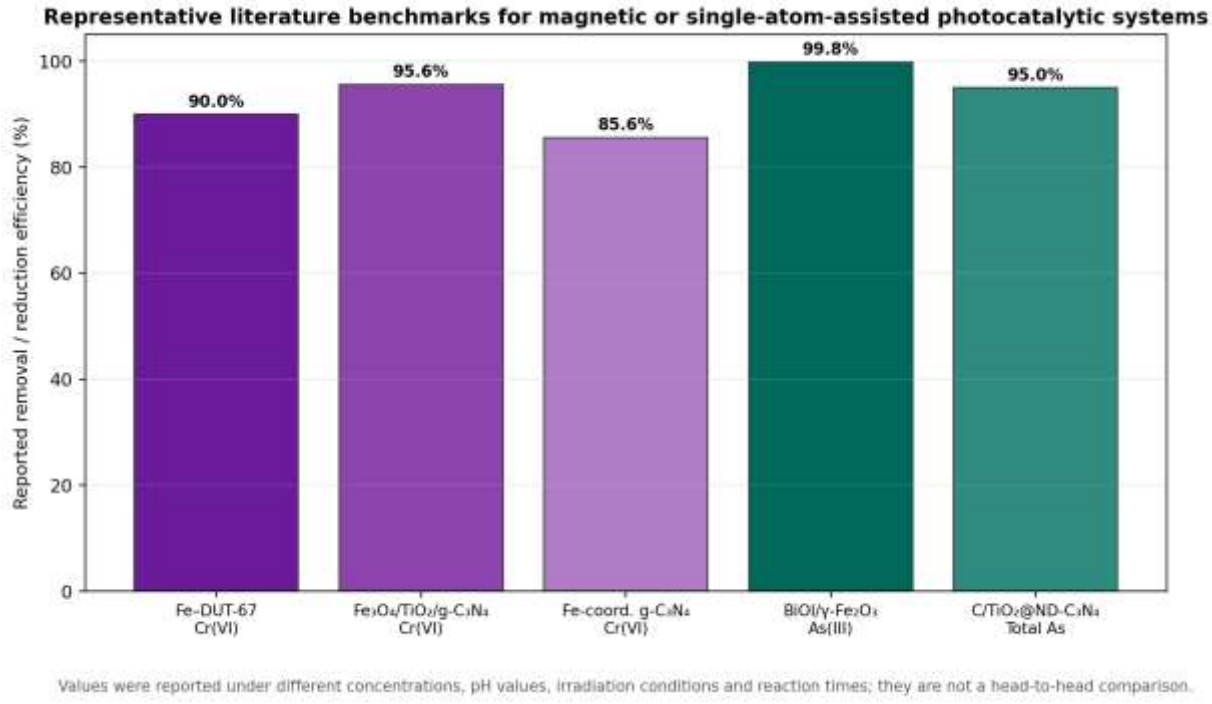

Figure 3. Representative performance values reported in selected primary studies. Bars are not a head-to-head ranking because experimental conditions differ substantially; they are included only to visualize the published

performance envelope for magnetic/Fe-modified Cr and arsenic photocatalytic systems [5,6,9,11,13].

5.11 Adsorption–photocatalysis synergy metrics

A useful way to quantify synergy is to partition removal into dark adsorption and light-dependent conversion. Let f_ads be the fraction removed during dark equilibration and f_photo the additional fraction removed after illumination, corrected for photolysis. A simple synergy index can compare the observed illuminated composite performance with the sum of independently measured adsorption and photochemical contributions, but such an index should be interpreted cautiously because adsorption changes local reactant activity. More mechanistically, one can correlate surface coverage with k_app or initial electron-equivalent rate. A positive relationship at low coverage followed by saturation would be consistent with a finite population of reactive adsorbed complexes.

$$S = R_{composite} / (R_{adsorption} + R_{photochemical,control}) \quad (10)$$

Operational synergy index S; values above unity indicate non-additive enhancement, provided all rates are measured under matched conditions.

5.12 Competing ions and natural organic matter

Phosphate is expected to be a particularly strong competitor for arsenate on Fe-containing surfaces because both form inner-sphere complexes. Bicarbonate can alter pH and radical chemistry, sulfate and nitrate affect ionic strength and may participate in photochemistry under some conditions, while natural organic matter can either consume holes beneficially or shield light and occupy adsorption sites. The sign of the organic-matter effect may therefore change with concentration. Matrix tests should report dissolved organic carbon and UV absorbance so that optical screening can be distinguished from chemical inhibition.

5.13 Reusability, iron leaching, and magnetic recovery

A reusable catalyst must retain three properties simultaneously: redox activity, adsorption capacity, and magnetic separability. Recent Fe single-atom/carbon-nitride membrane work demonstrates that isolated Fe sites can be incorporated into practical water-treatment architectures and maintain function over repeated operation [15]. For the particulate composite proposed here, cycle-to-cycle data should include mass recovery, saturation magnetization, Fe leaching, and post-cycle FeSA structural evidence. A loss of activity accompanied by unchanged magnetization would point toward poisoning or FeSA reconstruction; a loss of magnetization would suggest magnetite dissolution/detachment; rising Fe in solution would undermine the heterogeneous-catalyst claim.

6. Environmental and Engineering Implications

The proposed FeSA–CN/Fe_3O_4 concept is attractive because it addresses a recurring trade-off in nanomaterial water treatment: high interfacial reactivity versus recoverability. Atomically dispersed active sites maximize metal utilization, whereas magnetic nanoparticles provide a practical separation handle. If the two Fe populations are spatially and analytically controlled, the composite can combine nanoscale charge-transfer chemistry with centimeter-scale magnetic handling. This is particularly relevant for batch polishing, recirculating photoreactors, or magnetically retained beds where free nanoparticle discharge is unacceptable.

6.1 Scale-up criteria

Scale-up should be guided by areal photon utilization and treated-water productivity rather than catalyst activity per gram alone. g-C_3N_4 strongly scatters light, and Fe_3O_4 can introduce optical shielding at excessive loadings; therefore, catalyst concentration has an optimum beyond which more solid can lower the illuminated fraction. Reactor depth, mixing, photon path length, and spectral power distribution should be reported. Magnetic separation energy is likely modest compared with pressure-driven membrane separation, but this benefit disappears if fine particles escape or if repeated magnetic harvesting causes aggregation and loss of accessible surface area.

6.2 Limitations and falsification criteria

- Single-atom identity may be obscured by the intentional presence of Fe_3O_4; inadequate spectroscopy could overstate the role of FeSA.

- As(V) reduction can generate As(III). Any condition that accumulates aqueous As(III) should be considered a treatment failure unless a downstream capture barrier is demonstrated.
- High removal percentage can arise from adsorption alone. Oxidation-state-resolved mass balance is required before claiming photocatalytic reduction.
- Sacrificial hole donors can artificially enhance rates and may create secondary organic contamination; practical operation should minimize or eliminate them.
- Acidic conditions favorable for oxyanion uptake/reduction can increase Fe dissolution. Leaching and structural stability must be measured across cycles.
- Cross-study benchmark values are not directly comparable because operational conditions differ; only matched internal controls can establish catalyst superiority.

7. Conclusions

This manuscript defines a chemically rigorous route for evaluating single-atom anchored magnetic nanocomposites for coupled oxyanion adsorption and in-situ photoreduction. The proposed FeSA–CN/Fe_3O_4 architecture assigns distinct but complementary functions to atomically dispersed Fe–N_x sites, the g-C_3N_4 semiconductor, and magnetite. For Cr(VI), the desired sequence is adsorption followed by multielectron reduction to Cr(III) and surface immobilization. For As(V), reductive treatment is fundamentally more demanding: safe operation requires oxygen exclusion, efficient electron supply, speciation-resolved monitoring of As(III), and evidence that reduction proceeds toward a retained As(0)-like state rather than stopping at the more mobile trivalent form. The most important experimental contribution would therefore be mechanistic, not merely numerical—demonstrating that atomic-site engineering increases photon-to-oxyanion electron transfer while magnetic integration enables recovery without destroying the isolated active centers.

If validated, the platform could provide a modular strategy for water matrices where adsorption alone is vulnerable to desorption and conventional photocatalysis suffers from poor catalyst recovery. The study should be judged by closed Cr/As mass balances, oxidation-state-resolved products, matched component controls, photon-normalized kinetics, Fe leaching, and multi-cycle magnetic recovery. Those criteria transform the title from a broad materials claim into a falsifiable environmental-chemistry research program.

References

[1] H. Yang, W.-Y. Lin, K. Rajeshwar, “Homogeneous and heterogeneous photocatalytic reactions involving As(III) and As(V) species in aqueous media,” Journal of Photochemistry and Photobiology A: Chemistry 123 (1999) 137–143. https://doi.org/10.1016/S1010-6030(99)00052-0.

[2] D. Monllor-Satoca, R. Gómez, W. Choi, “Concentration-Dependent Photoredox Conversion of As(III)/As(V) on Illuminated Titanium Dioxide Electrodes,” Environmental Science & Technology 46 (2012) 5519–5527. https://doi.org/10.1021/es203922g.

[3] M. Bissen, M.M. Vieillard-Baron, A.J. Schindelin, F.H. Frimmel, “TiO_2-catalyzed photooxidation of arsenite to arsenate in aqueous samples,” Chemosphere 44 (2001) 751–757. https://doi.org/10.1016/S0045-6535(00)00489-6.

[4] J.-G. Kim, H.-B. Kim, G.-S. Yoon, S.-H. Kim, S.-J. Min, D.C.W. Tsang, K. Baek, “Simultaneous oxidation and adsorption of arsenic by one-step fabrication of alum sludge and graphitic carbon nitride (g-C_3N_4),” Journal of Hazardous Materials 383 (2020) 121138. https://doi.org/10.1016/j.jhazmat.2019.121138.

[5] Y. Wang, X. Liu, Q. Chen, T.C. Zhang, L. Ouyang, S. Yuan, “Simultaneous photocatalytic oxidation and adsorption for efficient As(III) removal by magnetic BiOI/γ-Fe_2O_3 core–shell nanoparticles,” Materials Today Chemistry 24 (2022) 100823. https://doi.org/10.1016/j.mtchem.2022.100823.

[6] H. Liu, Z. Yu, M. Xiao, W. Zhu, J. Liu, L. Wang, T. Xu, W. Wang, T. Yang, "Synergistic photocatalytic oxidation and adsorption boost arsenic removal by in-situ carbon-doped TiO_2 and nitrogen deficiency C_3N_4 heterojunction," Journal of Environmental Management 348 (2023) 119218. https://doi.org/10.1016/j.jenvman.2023.119218.

[7] X. Ding, D. Xiao, L. Ji, D. Jin, K. Dai, Z.X. Yang, S.Y. Wang, H. Chen, "Simple fabrication of Fe_3O_4/C/g-C_3N_4 two-dimensional composite by hydrothermal carbonization approach with enhanced photocatalytic performance under visible light," Catalysis Science & Technology 8 (2018) 3484–3492. https://doi.org/10.1039/C8CY00698A.

[8] T. Wang, L. Zheng, Y. Liu, W. Tang, T. Fang, B. Xing, "A novel ternary magnetic Fe_3O_4/g-C_3N_4/Carbon layer composite for efficient removal of Cr(VI): A combined approach using both batch experiments and theoretical calculation," Science of the Total Environment 730 (2020) 138928. https://doi.org/10.1016/j.scitotenv.2020.138928.

[9] N. Madima, K.K. Kefeni, A.T. Kuvarega, S.B. Mishra, A.K. Mishra, "Visible-light-driven Z-scheme ternary Fe_3O_4/TiO_2/g-C_3N_4 nanocomposite as reusable photocatalyst for efficient removal of dyes and chromium in water," Materials Chemistry and Physics 296 (2023) 127233. https://doi.org/10.1016/j.matchemphys.2022.127233.

[10] X. Zhang, J. Liu, X. Zheng, R. Chen, M. Zhang, Z. Liu, Z. Wang, J. Li, "Activation of oxalic acid via dual-pathway over single-atom Fe catalysts: Mechanism and membrane application," Applied Catalysis B: Environmental 321 (2023) 122068. https://doi.org/10.1016/j.apcatb.2022.122068.

[11] H. Jia, J. Ye, S. Dong, Z. Zeng, D. Tang, X. Wang, S. Chen, "New insights into the mechanism for Fe coordination promoting photocatalytic reduction of Cr(VI) by graphitic carbon nitride: The boosted transformation of Cr(V) to Cr(III)," Applied Surface Science 679 (2025) 161142. https://doi.org/10.1016/j.apsusc.2024.161142.

[12] Z. Hu, Z. Liu, C.C. Tay, L. Bao, M. Qiu, "Investigating the photocatalytic reduction of U(VI) over a single-atom Fe complex catalyst," Journal of Molecular Liquids 411 (2024) 125774. https://doi.org/10.1016/j.molliq.2024.125774.

[13] Y. Xiang, X. Ji, X. Dong, Y. Wang, N. Zheng, J. Niu, P. Yu, C. Yan, "Fe single atom post-synthetic modification of DUT-67 for highly efficient photocatalytic reduction of Cr(VI)," Applied Surface Science 736 (2026) 166837. https://doi.org/10.1016/j.apsusc.2026.166837.

[14] L. Ye, X. Chen, Y. Huang, J. Zhang, Y. Li, C. Yang, B. Xiao, "Selective Remediation and Reduction of Cr(VI) to Cr(II) Using Carbon-Supported Co, Ni, and Zn Single-Atom Catalysts: A First-Principles Investigation," ACS Omega 10 (2025) 48005–48018. https://doi.org/10.1021/acsomega.5c03892.

[15] T. Bai, R. Zhang, S. Wei, B. Li, "Fabrication of multifunctional membranes via integrating g-C_3N_4 with Fe single-atom sites for efficient wastewater treatment," Environmental Research 301 (2026) 124501. https://doi.org/10.1016/j.envres.2026.124501.

[16] Z. Su, H. Long, S. Song, R.-R. Zhao, L. Zhou, A. Gao, K. Gao, W.-J. Xiao, "Atomically dispersed iron on carbon nitride with enhanced oxygen adsorption for efficient and scalable photooxidation," Nature Communications 17 (2026) 6999. https://doi.org/10.1038/s41467-026-73877-5.